Anti-plane problem of nano-cracks emanating from a regular hexagonal nano-hole in one-dimensional hexagonal piezoelectric quasicrystals*

Dongsheng Yang(杨东升) and Guanting Liu(刘官厅)†

College of Mathematics Science, Inner Mongolia Normal University, Hohhot 010022, *China*

(Received 19 March 2020; accepted manuscript online 18 June 2020)

By constructing a new conformal mapping function, we study the surface effects on six edge nano-cracks emanating from a regular hexagonal nano-hole in one-dimensional (1D) hexagonal piezoelectric quasicrystals under anti-plane shear. Based on the Gurtin–Murdoch surface/interface model and complex potential theory, the exact solutions of phonon field, phason field and electric field are obtained. The analytical solutions of the stress intensity factor of the phonon field, the stress intensity factor of the phason field, the electric displacement intensity factor and the energy release rate are given. The interaction effects of the nano-cracks and nano-hole on the stress intensity factor of the phonon field, the stress intensity factor of the phason field and the electric displacement intensity factor are discussed in numerical examples. It can be seen that the surface effect leads to the coupling of phonon field, phason field and electric field. With the decrease of cavity size, the influence of surface effect is more obvious.

Keywords: one-dimensional quasicrystals, piezoelectricity, surface effect; energy release rate

PACS: 46.05.+b, 46.25.–y, 46.50.+a **DOI:** 10.1088/1674-1056/ab9ddf

1. Introduction

Quasicrystals (QCs) are a kind of materials with new structures discovered in 1984.[1] Because of their defects (cracks, holes, dislocations, etc.), they are often characterized by brittle mechanics. It is easy to produce stress concentration to accelerate crack growth and even lead to structural damage under the action of the electromechanical coupling field. Therefore, it is of great significance for the study of quasicrystal fracture mechanics.

In the study of quasicrystal fracture mechanics, Liu *et al*.[2–4] introduced a new displacement potential function to obtain the control equation, which solved the plane elastic problem of two-dimensional QCs. A lot of research has been performed on defects of different shapes. Guo and Liu[5–7] have studied the exact solution to the problem of asymmetric cracks with circular and elliptical holes. Chen *et al*.[8] studied the exact solution to the circular hole problem with 2^K periodic radial cracks. Zhong and Liu[9] studied the analytical solution to the problem of lip defects in 1D hexagonal piezoelectric QCs. In Ref. [10] the authors studied the antiplane problem of asymmetric cracks in a hexagonal hole. In addition, the study of different types of defects in QCs has also attracted much attention. In Ref. [11], Liu and Yang gave the analytical solution of the generalized stress field of the interaction between infinite parallel screw dislocations and a semi-infinite crack in 1D hexagonal QCs. Li and Liu[12] deduced the stress intensity factor and dislocation force at the crack tip when a screw dislocation interacts with a semi-infinite wedge-shaped crack in 1D hexagonal QCs. In addition, Li and Liu have studied the analytical solution of the interaction between dislocation and elliptical holes in 1D hexagonal QCs.[13] The dynamic problem of defects in 1D hexagonal piezoelectric QCs has also been studied a lot. In Refs. [14,15], the problems of dynamic screw dislocation and moving crack in 1D hexagonal piezoelectric QCs are studied, and the analytical solutions of stress and displacement fields are derived respectively.

When the size of hole and cracks is at nanoscales, the sizes of hole and cracks are very small, and the ratio of surface area to volume is very large. At this time, the stress field around the hole and the stress intensity factor at the crack tip show obvious scale effects.[16,17] The Gurtin–Murdoch surface/interface model[18,19] considered the influence of surface free energy by introducing surface stress and described the macroscopic characteristic sizes of continuum mechanics and the microscopic characteristic sizes of nano defects. This theory is widely used in research of fracture behavior of nanoscale defects. Xiao *et al*.[20] studied the problem of triangular nano-hole with nano-cracks in piezoelectric body under the impermeable boundary condition, and obtained the analytical solutions of the intensity factor of the electroelastic field and the energy release rate at the crack tip. Guo and Li[21] studied the problem of nano-hole or nano-cracks in piezoelectric body under the permeable boundary, and obtained the ana-

*Project supported by the National Key R&D Program of China (Grant No. 2017YFC1405605), the Innovation Youth Fund of the Ocean Telemetry Technology Innovation Center of the Ministry of Natural Resources, China (Grant No. 21k20190088), the Natural Science Foundation of Inner Mongolia, China (Grant No. 2018MS01005), and the Graduate Students' Scientific Research Innovation Program of Inner Mongolia Normal University (Grant No. CXJJS19098).

†Corresponding author. E-mail: guantingliu@imnu.edu.cn

lytical solutions of stress field and electric field. The antiplane problem of elliptical nano-hole in magnetoelectroelastic materials has also been reported.[22,23]

The problem of regular hexagonal hole with cracks widely exists in engineering. In Ref. [24], the stress distribution around the regular hexagon hole of the boat hull structure was studied, which has important engineering significance. Due to good seismic performance of the hexagonal honeycomb members,[25] the hexagonal honeycomb beams are widely used at present. However, due to the phenomenon of stress concentration, cracks are easy to occur at the hole edge. Therefore, it is very important to study the stress intensity factor of regular hexagon hole and cracks. In Ref. [10], a conformal mapping from a regular hexagon hole with double cracks to a unit circle was constructed, and an analytical solution of the stress intensity factor was obtained using the complex method.

In this paper, a new conformal mapping is constructed, the exterior of the regular hexagonal nano-hole with six nano-cracks in the z plane is mapped to the interior of the circle with radius a in the ζ plane. Based on the Gurtin–Murdoch surface/interface model and the complex method, the electrically impermeable boundary conditions are established via considering the influence of surface effect. The analytical solutions of phonon field, phason field and electric field of holes with edge cracks at nanoscales are obtained. In the part of numerical analysis, we depict the effects of nano-cracks and nano-holes on the stress intensity factor of the phonon field, the stress intensity factor of the phason field and the electric displacement intensity factor. In addition, the effects of mechanical loads of phonon field, mechanical loads of phason field and electrical loads on the energy release rate are also discussed.

2. Basic equations

In this paper, 1D hexagonal piezoelectric QCs with defects at nanoscales are studied. As shown in Fig. 1, the shape of defects is a hexagonal hole with six equal length cracks. The hexagonal side length is a, the crack length is L, and the defect penetrates along the quasi-periodic direction. It is affected by the phonon field τ_{zy}^{∞}, the phason field H_{zy}^{∞} and the electric field D_y^{∞} at infinity. For 1D hexagonal piezoelectric QCs, we take the z-axis as the quasi-periodic direction and the electrode direction, and select the xoy plane perpendicular to the z-axis as the isotropic plane. The constitutive relation can be expressed as follows:

$$\begin{aligned}
\sigma_{zx} &= 2c_{44}\varepsilon_{zx} + R_3\omega_{zx} - e_{15}E_x,\\
\sigma_{zy} &= 2c_{44}\varepsilon_{zy} + R_3\omega_{zy} - e_{15}E_y,\\
H_{zx} &= 2R_3\varepsilon_{zx} + K_2\omega_{zx} - d_{15}E_x,\\
H_{zy} &= 2R_3\varepsilon_{zy} + K_2\omega_{zy} - d_{15}E_y,\\
D_x &= 2e_{15}\varepsilon_{zx} + d_{15}\omega_{zx} + \lambda_{11}E_x,\\
D_y &= 2e_{15}\varepsilon_{zy} + d_{15}\omega_{zy} + \lambda_{11}E_y.
\end{aligned} \tag{1}$$

Regardless of body force and electric charge density, the static equilibrium equation of 1D hexagonal piezoelectric QCs is as follows:

$$\sigma_{zj,j} = 0, \quad H_{zj,j} = 0, \quad D_{j,j} = 0. \tag{2}$$

The gradient equations is

$$\varepsilon_{zj} = \frac{1}{2}u_{z,j}, \quad \omega_{zj} = w_{z,j}, \quad E_j = -\varphi_{,j}, \tag{3}$$

where $j = x, y$ in Cartesian coordinates; σ_{zj}, ε_{zj} and u_z represent the stress, strain and displacement of the phonon field respectively; H_{zj}, ω_{zj} and w_z represent the stress, strain and displacement of the phason field; D_j, E_j and φ are the potential shift, electric field and potential; c_{44} is the elastic constant of the phonon field; K_2 is the elastic constant of the phason field; R_3 is the coupling constant of the phonon field and the phason field; e_{15} is the piezoelectric constant of the phonon field; d_{15} is the piezoelectric constant of the phason field; λ_{11} is the dielectric constant.

The material matrix $\boldsymbol{A}$ and the generalized displacement $\boldsymbol{u}$ are defined as follows:

$$\boldsymbol{A} = \begin{bmatrix} c_{44} & R_3 & e_{15} \\ R_3 & K_2 & d_{15} \\ e_{15} & d_{15} & -\lambda_{11} \end{bmatrix}, \quad \boldsymbol{u} = \begin{bmatrix} u_z & \omega_z & \varphi \end{bmatrix}^{\mathrm{T}}. \tag{4}$$

$\boldsymbol{A}$ in the above formula is nonsingular, and the superscript T denotes the transpose of the vector or matrix. According to formulae (1)–(3), we can obtain

$$\nabla^2 \boldsymbol{u} = \boldsymbol{0}, \tag{5}$$

where ∇^2 is the Laplace operator.

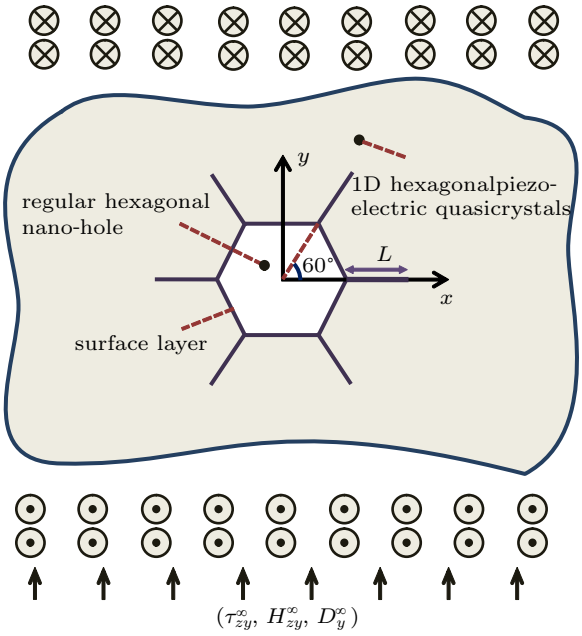

Fig. 1. Regular hexagonal nano-hole with six nano-cracks in 1D hexagonal piezoelectric QCs.

According to the method of the complex variable function, the solutions u_3, w_3 and φ of harmonic Eq. (5) can be expressed as the real part or imaginary part of three analytic functions $F_1(z)$, $F_2(z)$ and $F_3(z)$. We can assume

$$\begin{aligned}\boldsymbol{u} &= \left[\, u_z \;\; \omega_z \;\; \varphi \,\right]^{\mathrm{T}} \\ &= \mathrm{Re}\left[\, F_1(z) \;\; F_2(z) \;\; F_3(z) \,\right]^{\mathrm{T}} = \mathrm{Re}\boldsymbol{F},\end{aligned} \tag{6}$$

where $z = x + \mathrm{i}y$, Re represents the real part of a complex function.

Since $F_i(z)$ $(i = 1,2,3)$ are analytical functions, we can obtain

$$\frac{\partial \boldsymbol{F}}{\partial x} = \boldsymbol{F}', \quad \frac{\partial \boldsymbol{F}}{\partial y} = \mathrm{i}\boldsymbol{F}', \tag{7}$$

where $F' = \mathrm{d}F/\mathrm{d}z$.

According to the above results, we have

$$\left[\;\; \sigma_{zx} - \mathrm{i}\sigma_{zy} \quad H_{zx} - \mathrm{i}H_{zy} \quad D_x - \mathrm{i}D_y \;\;\right]^{\mathrm{T}} = \boldsymbol{A}\boldsymbol{F}'. \tag{8}$$

The above formula can be expressed by polar coordinates

$$\left[\;\; \sigma_{z\theta} - \mathrm{i}\sigma_{zr} \quad H_{z\theta} - \mathrm{i}H_{zr} \quad D_\theta - \mathrm{i}D_r \;\;\right]^{\mathrm{T}} = \mathrm{e}^{\mathrm{i}\theta}\boldsymbol{A}\boldsymbol{F}'. \tag{9}$$

3. Analytical solution under the boundary condition of electric impermeability

Define $\boldsymbol{A}^{\mathrm{s}}$ as the surface constant matrix,

$$\boldsymbol{A}^{\mathrm{s}} = \begin{bmatrix} c_{44}^{\mathrm{s}} & R_3^{\mathrm{s}} & e_{15}^{\mathrm{s}} \\ R_3^{\mathrm{s}} & K_2^{\mathrm{s}} & d_{15}^{\mathrm{s}} \\ e_{15}^{\mathrm{s}} & d_{15}^{\mathrm{s}} & -\lambda_{11}^{\mathrm{s}} \end{bmatrix}, \tag{10}$$

where c_{44}^{s} is the surface elastic constant of the phonon field, K_2^{s} is the surface elastic constant of the phason field, R_3^{s} is the coupling surface constant of the phonon field and the phason field, e_{15}^{s} is the surface piezoelectric constant of the phonon field, d_{15}^{s} is the surface piezoelectric constant of the phason field, and $\lambda_{11}^{\mathrm{s}}$ is the surface dielectric constant.

Based on the Gurtin–Murdoch theory of surface elasticity, hexagonal nano-hole with six nano-cracks in 1D hexagonal piezoelectric QCs are considered. The boundary conditions of the defects at nanoscales are as follows:

$$\begin{aligned} & u_z^{\mathrm{c}}(t) = u_z^{\mathrm{m}}(t), \;\; w_z^{\mathrm{c}}(t) = w_z^{\mathrm{m}}(t), \;\; \varphi^{\mathrm{c}}(t) = \varphi^{\mathrm{m}}(t), \\ & -\left[\, \sigma_{zr}^{\mathrm{m}}(t) \;\; H_{zr}^{\mathrm{m}}(t) \;\; D_r^{\mathrm{m}}(t) \,\right]^{\mathrm{T}} \end{aligned} \tag{11}$$

$$= \frac{\boldsymbol{A}^{\mathrm{s}}}{\rho}\left[\, \varepsilon_{z\theta,\theta}^0 \;\; \omega_{z\theta,\theta}^0 \;\; -E_{\theta,\theta}^0 \,\right]^{\mathrm{T}}, \tag{12}$$

where the superscripts c, m, and s refer to quantities for the nano-hole, matrix, and surface of nano-hole, respectively; $\varepsilon_{z\theta}^0$ is the surface strain component of phonon field, $w_{z\theta}^0$ is the surface strain component of phason field, E_θ^0 is the surface potential component, and (ρ, θ) is the polar coordinate.

In order to solve this boundary value problem, inspired Ref. [10], the following conformal mapping is constructed. The exterior of the regular nano-hexagon with six nano-cracks in the z plane is mapped to the interior of the circle with radius a in the ζ plane. The construction process is detailedly described in the appendix. We have

$$\begin{aligned} z &= \omega(\zeta) = R[\mu(\zeta) + \frac{1}{15}\mu(\zeta)^{-5} \\ &\quad + \frac{1}{99}\mu(\zeta)^{-11} + \frac{1}{1377}\mu(\zeta)^{-17}], \end{aligned} \tag{13}$$

$$\begin{aligned} \mu(\zeta) &= \frac{1}{2^{\frac{1}{3}}\zeta a}[(\zeta^6 - a^6)^2 + l(\zeta^6 + a^6)^2 + \sqrt{1+l}(\zeta^6 + a^6) \\ &\quad \times \sqrt{(1+l)\zeta^{12} + 2(l-3)\zeta^6 a^6 + (1+l)a^{12}}]^{\frac{1}{6}}, \end{aligned} \tag{14}$$

where R is a constant coefficient related to the side length of a regular hexagon, $R = 0.9258a$, $l = [(1+c)^6 + (1+c)^{-6}]/2$. The positive real parameter c determined by the following formula:

$$\begin{aligned} L + a &= R\left[(1+c) + \frac{1}{15}(1+c)^{-5} + \frac{1}{99}(1+c)^{-11} \right. \\ &\quad \left. + \frac{1}{1377}(1+c)^{-17}\right]. \end{aligned} \tag{15}$$

The analytic functions $F_i(z)$ $(i = 1,2,3)$ are expanded to Laurent series in ζ plane

$$F_i(\zeta) = a_i^* \ln\zeta + \sum_{-\infty}^{+\infty} a_{ik}\zeta^k \quad (i = 1,2,3), \tag{16}$$

where a_i^* and a_{ik} are undetermined constants, according to Ref. [18], the solutions to the problem can be obtained by selecting the finite term

$$\boldsymbol{F}^c(\zeta) = \begin{bmatrix} F_1^c(\zeta) \\ F_2^c(\zeta) \\ F_3^c(\zeta) \end{bmatrix} = \begin{bmatrix} A_1 \\ C_1 \\ E_1 \end{bmatrix}\zeta, \tag{17}$$

$$\boldsymbol{F}^{\mathrm{m}}(\zeta) = \begin{bmatrix} F_1^{\mathrm{m}}(\zeta) \\ F_2^{\mathrm{m}}(\zeta) \\ F_3^{\mathrm{m}}(\zeta) \end{bmatrix} = \begin{bmatrix} B_1 \\ D_1 \\ F_1 \end{bmatrix}\zeta + \begin{bmatrix} B_{-1} \\ D_{-1} \\ F_{-1} \end{bmatrix}\zeta^{-1}, \tag{18}$$

where $\boldsymbol{F}^c(\zeta)$ is the analytic function matrix inside the circle, $\boldsymbol{F}^{\mathrm{m}}(\zeta)$ is the analytic function matrix outside the circle, and A_1, B_1, C_1, D_1, E_1, F_1, B_{-1}, D_{-1} and F_{-1} are complex constants.

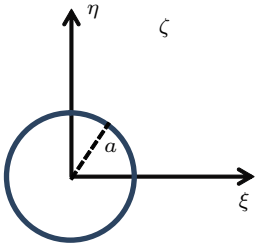

Fig. 2. Conformal mapping ($\zeta = \xi + \mathrm{i}\eta$).

Substituting Eq. (18) into Eq. (8) and considering the loads at infinity yield

$$\begin{bmatrix} B_1 \\ D_1 \\ F_1 \end{bmatrix} = -\mathrm{i}\frac{(1+l)^{\frac{1}{6}}R}{2^{\frac{1}{6}}a}\boldsymbol{A}^{-1}\begin{bmatrix} \tau_{zy}^{\infty} \\ H_{zy}^{\infty} \\ D_y^{\infty} \end{bmatrix}. \tag{19}$$

On the defect surface, according to boundary conditions (11) and Eq. (12), we can reach

$$\begin{bmatrix} A_1 \\ C_1 \\ E_1 \end{bmatrix} = \begin{bmatrix} B_1 \\ D_1 \\ F_1 \end{bmatrix} - \frac{1}{a^2}\begin{bmatrix} B_{-1} \\ D_{-1} \\ F_{-1} \end{bmatrix}, \tag{20}$$

$$\frac{\boldsymbol{A}^{\mathrm{s}}}{a}\begin{bmatrix} A_1 \\ C_1 \\ E_1 \end{bmatrix} = \boldsymbol{A}\left\{\begin{bmatrix} B_1 \\ D_1 \\ F_1 \end{bmatrix} + \frac{1}{a^2}\begin{bmatrix} B_{-1} \\ D_{-1} \\ F_{-1} \end{bmatrix}\right\}. \tag{21}$$

The following results can be obtained by combining the above two formulas:

$$\begin{bmatrix} B_{-1} \\ D_{-1} \\ F_{-1} \end{bmatrix} = \mathrm{i}\frac{(1+l)^{\frac{1}{6}}Ra}{2^{\frac{1}{6}}}\left(\frac{\boldsymbol{A}^{\mathrm{s}}}{a}+\boldsymbol{A}\right)^{-1} \times\left(\boldsymbol{A}-\frac{\boldsymbol{A}^{\mathrm{s}}}{a}\right)\boldsymbol{A}^{-1}\begin{bmatrix} \tau_{zy}^{\infty} \\ H_{zy}^{\infty} \\ D_{y}^{\infty} \end{bmatrix}. \tag{22}$$

Substituting the above results into Eq. (8), the results are as follows:

$$\begin{bmatrix} \sigma_{zy} \\ H_{zy} \\ D_y \end{bmatrix} = \frac{(1+l)^{\frac{1}{6}}R}{2^{\frac{1}{6}}\omega'(\zeta)a}\left[\boldsymbol{E}-\frac{a^2\boldsymbol{A}}{\zeta^2}\left(\frac{\boldsymbol{A}^{\mathrm{s}}}{a}+\boldsymbol{A}\right)^{-1} \times\left(\frac{\boldsymbol{A}^{\mathrm{s}}}{a}-\boldsymbol{A}\right)\boldsymbol{A}^{-1}\right]\begin{bmatrix} \tau_{zy}^{\infty} \\ H_{zy}^{\infty} \\ D_{y}^{\infty} \end{bmatrix}, \tag{23}$$

where $\boldsymbol{E}$ is the third-order unit matrix.

4. Field intensity factor and energy release rate

4.1. Field intensity factor

The stress of the phonon field, the stress of the phason field and the electric displacement intensity factors at the crack tip can be defined as[18]

$$\begin{bmatrix} K_{\mathrm{III}}^{\sigma} \\ K_{\mathrm{III}}^{H} \\ K_{\mathrm{III}}^{D} \end{bmatrix} = \lim_{z\to z_0}\sqrt{2\pi(z-z_0)}\begin{bmatrix} \sigma_{zy} \\ H_{zy} \\ D_y \end{bmatrix}. \tag{24}$$

Conformal mapping maps crack tip $z=L+a$ in z plane to $\zeta=a$ in ζ plane, and substituting Eq. (23) into Eq. (24) yields

$$\begin{bmatrix} K_{\mathrm{III}}^{\sigma} \\ K_{\mathrm{III}}^{H} \\ K_{\mathrm{III}}^{D} \end{bmatrix} = \frac{\sqrt{\pi}(1+l)^{\frac{1}{6}}R}{2^{\frac{1}{6}}\sqrt{\omega''(a)a}}\left[\boldsymbol{E}-\boldsymbol{A}\left(\frac{\boldsymbol{A}^{\mathrm{s}}}{a}+\boldsymbol{A}\right)^{-1} \times\left(\frac{\boldsymbol{A}^{\mathrm{s}}}{a}-\boldsymbol{A}\right)\boldsymbol{A}^{-1}\right]\begin{bmatrix} \tau_{zy}^{\infty} \\ H_{zy}^{\infty} \\ D_{y}^{\infty} \end{bmatrix}. \tag{25}$$

Suppose Eq. (25) can be expressed as

$$\begin{bmatrix} K_{\mathrm{III}}^{\sigma} \\ K_{\mathrm{III}}^{H} \\ K_{\mathrm{III}}^{D} \end{bmatrix} = \frac{\sqrt{\pi}(1+l)^{\frac{1}{6}}R}{2^{\frac{1}{6}}\sqrt{\omega''(a)a}}\begin{bmatrix} K_{\tau}^{*} \\ K_{H}^{*} \\ K_{D}^{*} \end{bmatrix}, \tag{26}$$

where

$$\begin{bmatrix} K_{\tau}^{*} \\ K_{H}^{*} \\ K_{D}^{*} \end{bmatrix} = \left[\boldsymbol{E}-\boldsymbol{A}\left(\frac{\boldsymbol{A}^{\mathrm{s}}}{a}+\boldsymbol{A}\right)^{-1} \times\left(\frac{\boldsymbol{A}^{\mathrm{s}}}{a}-\boldsymbol{A}\right)\boldsymbol{A}^{-1}\right]\begin{bmatrix} \tau_{zy}^{\infty} \\ H_{zy}^{\infty} \\ D_{y}^{\infty} \end{bmatrix}. \tag{27}$$

When the material constant matrix $\boldsymbol{A}^{\mathrm{s}}=\boldsymbol{0}$, Eq. (27) degenerates to the classical field intensity factor of 1D hexagonal piezoelectric QCs,

$$\begin{bmatrix} K_{\mathrm{III}}^{\sigma} \\ K_{\mathrm{III}}^{H} \\ K_{\mathrm{III}}^{D} \end{bmatrix} = \frac{2\sqrt{\pi}(1+l)^{\frac{1}{6}}R}{2^{\frac{1}{6}}\sqrt{\omega''(a)a}}\begin{bmatrix} \tau_{zy}^{\infty} \\ H_{zy}^{\infty} \\ D_{y}^{\infty} \end{bmatrix}, \tag{28}$$

which is the same as the previous results,[9] except for conformal mapping. It can be seen that under the influence of surface effect, $K_{\mathrm{III}}^{\sigma}$, K_{III}^{H} and K_{III}^{D} are related to the surface constants and are determined by τ_{zy}^{∞}, H_{zy}^{∞} and D_{y}^{∞}, which is obviously different from the results not affected by surface effect.

The above formula can be rewritten as

$$\begin{bmatrix} K_{\mathrm{III}}^{\sigma} \\ K_{\mathrm{III}}^{H} \\ K_{\mathrm{III}}^{D} \end{bmatrix} = \sqrt{\pi L'}K\begin{bmatrix} \tau_{zy}^{\infty} \\ H_{zy}^{\infty} \\ D_{y}^{\infty} \end{bmatrix}, \tag{29}$$

where $L'=L+a$, K is a dimensionless field intensity factor, and $K=\frac{2(1+l)^{\frac{1}{6}}R}{2^{\frac{1}{6}}\sqrt{L'\omega''(a)a}}$.

4.2. Energy release rate

For impermeable cracks, the formula of energy release rate is

$$J=\frac{1}{2}\begin{bmatrix} K_{\mathrm{III}}^{\sigma} & K_{\mathrm{III}}^{H} & K_{\mathrm{III}}^{D} \end{bmatrix}\boldsymbol{A}^{-1}\begin{bmatrix} K_{\mathrm{III}}^{\sigma} \\ K_{\mathrm{III}}^{H} \\ K_{\mathrm{III}}^{D} \end{bmatrix}. \tag{30}$$

By substituting Eq. (25) into Eq. (31), the energy release rate of 1D hexagonal piezoelectric QCs with hexagonal hole and six cracks under the influence of surface effect can be expressed as

$$\begin{aligned} J = {} & \frac{\pi(1+l)^{\frac{1}{3}}R^2}{2\times 2^{\frac{1}{3}}\omega''(a)a^2}\begin{bmatrix} \tau_{zy}^{\infty} \\ H_{zy}^{\infty} \\ D_{y}^{\infty} \end{bmatrix}^{\mathrm{T}} \\ & \times\left[\boldsymbol{E}-\boldsymbol{A}\left(\frac{\boldsymbol{A}^{\mathrm{s}}}{a}+\boldsymbol{A}\right)^{-1}\left(\frac{\boldsymbol{A}^{\mathrm{s}}}{a}-\boldsymbol{A}\right)\boldsymbol{A}^{-1}\right]^{\mathrm{T}} \\ & \times\left[\boldsymbol{A}^{-1}-\left(\frac{\boldsymbol{A}^{\mathrm{s}}}{a}+\boldsymbol{A}\right)^{-1}\left(\frac{\boldsymbol{A}^{\mathrm{s}}}{a}-\boldsymbol{A}\right)\boldsymbol{A}^{-1}\right] \\ & \times\begin{bmatrix} \tau_{zy}^{\infty} \\ H_{zy}^{\infty} \\ D_{y}^{\infty} \end{bmatrix}. \end{aligned} \tag{31}$$

Especially, by substituting Eq. (29) into Eq. (31), the energy release rate of a classical 1D hexagonal piezoelectric QCs

can be expressed as

$$J=\frac{2\pi(1+l)^{\frac{1}{3}}R^2}{2^{\frac{1}{3}}\omega''(a)a^2\det A}\Lambda, \tag{32}$$

where

$$\begin{aligned}\Lambda &= (d_{15}^2+K_2\lambda_{11})(\tau_{zy}^{\infty})^2+(e_{15}^2+c_{44}\lambda_{11})(H_{zy}^{\infty})^2\\ &+(R_3^2-K_2c_{44})(D_y^{\infty})^2+2(e_{15}K_2\\ &-d_{15}R_3)\tau_{zy}^{\infty}H_{zy}^{\infty}+2(c_{44}d_{15}-e_{15}R_3)H_{zy}^{\infty}D_y^{\infty}\\ &-(d_{15}e_{15}+\lambda_{11}R_3)\tau_{zy}^{\infty}H_{zy}^{\infty}.\end{aligned} \tag{33}$$

5. Numerical analysis

The material constants[26] are selected as follows: $c_{44}=50$ GPa, $R_3=1.2$ GPa, $K_2=0.3$ GPa, $e_{15}=-0.138$ C/m^2, $d_{15}=-0.160$ C/m^2 and $\lambda_{11}=82.6\times10^{-12}$ C^2·N/m^2. We choose $c_{44}^{\rm s}=62.5$ N/m, $R_3^{\rm s}=1.5$ N/m, $K_2^{\rm s}=0.5$ N/m, $e_{15}^{\rm s}=1.25\times10^{-8}$ C/m, $d_{15}^{\rm s}=0.62\times10^{-8}$ C/m and $\lambda_{11}^{\rm s}=0$ as an approximation according to reasonable estimates for some metal surfaces. It can be seen that K_τ^*,K_H^*,K_D^* is affected by the material, radius a and load. When the surface effect is not considered, substituting $\boldsymbol{A}^{\rm s}=\boldsymbol{0}$ into Eq. (28) yields

$$\begin{bmatrix}K_\tau^*\\K_H^*\\K_D^*\end{bmatrix}=\begin{bmatrix}2&0&0\\0&2&0\\0&0&2\end{bmatrix}\begin{bmatrix}\tau_{zy}^{\infty}\\H_{zy}^{\infty}\\D_y^{\infty}\end{bmatrix}, \tag{34}$$

which is the same as the results of Zhong *et al.*[9]

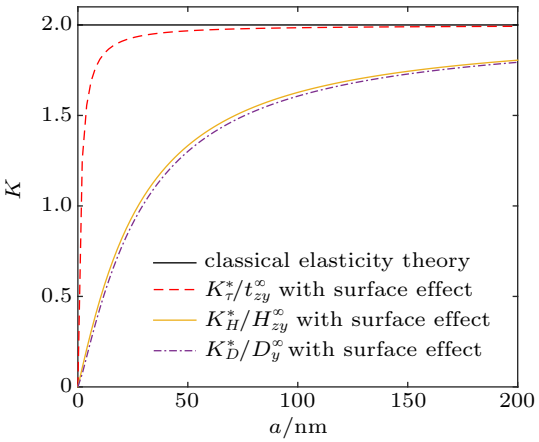

Fig. 3. With surface effect: when only the phonon field stress is applied, variations of $K_\tau^*/\tau_{zy}^{\infty}$ with a; when only the phason field stress is applied, variations of K_H^*/H_{zy}^{∞} with a; when only the electric field stress is applied, variations of K_D^*/D_y^{∞} with a. Without surface effect: classical elasticity theory.

It can be seen that the values of $K_\tau^*/\tau_{zy}^{\infty}$, K_H^*/H_{zy}^{∞} and K_D^*/D_y^{∞} are equal without surface effect. Figure 3 shows that the values of $K_\tau^*/\tau_{zy}^{\infty}$, K_H^*/H_{zy}^{∞} and K_D^*/D_y^{∞} affected by the surface effect gradually increase with the increase of a, and finally tend to 2. However, this is not enough to draw a conclusion. After analyzing Figs. 4–9, we can see that the values of variables in the figures all tend to 0. Therefore, it can be concluded that with the increase of length of nano-cracks, the influence of surface effect begins to decrease and finally tends to the classical fracture theory. It can be observed from Figs. 4 and 5 that the stress intensity factor of the phonon field with surface effect is dependent on the electrical loads and phason field mechanical loads. Figures 6 and 7 show that the stress intensity factor of the phason field with surface effect is dependent on the electrical loads and phonon field mechanical loads. Figures 8 and 9 show that the electric displacement intensity factor with surface effect is dependent on the phonon field mechanical loads and phason field mechanical loads, which is different from the classical elasticity result. In other words, the surface effect can result in the coupling of electric field, phonon field and phason field. Figure 10 shows the influence of length of nano-cracks on the dimensionless field intensity factor. It can be seen from the figure that with the increase of crack length, the dimensionless field intensity factor increases gradually, and in a certain range, the smaller the side length of hexagon is, the larger the value of K is.

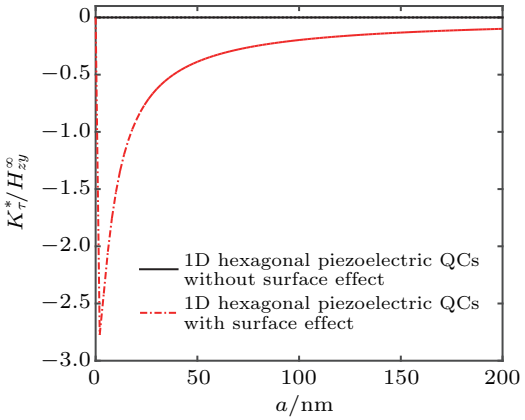

Fig. 4. Variations of K_τ^*/H_{zy}^{∞} with a.

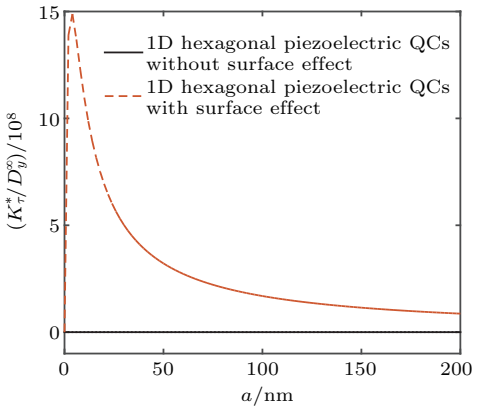

Fig. 5. Variations of K_τ^*/D_y^{∞} with a.

Figure 11 shows the curve of crack tip normalized energy release rate $J/J_{\rm cr}$ with phonon field mechanical loads τ_{zy}^{∞}, where $a=5$ nm, $L=a$. It is shown that the normalized energy release first decreases and then increases with the increase of τ_{zy}^{∞} from 0 MPa to 30 MPa. The law of variation is similar to that of piezoelectric materials.[18] Figure 12 shows the curve of crack tip normalized energy release rate $J/J_{\rm cr}$ with

phason field mechanical loads H_{zy}^{∞}, where $a = 5$ nm, $L = a$. It is shown that the normalized energy release first decreases and then increases as the phason field mechanical loads H_{zy}^{∞} increases from 0 MPa to 10 MPa. Proper increase of electrical loads will increase the energy release rate. Figure 13 shows the curve of crack tip normalized energy release rate $J/J_{\rm cr}$ with electrical loads D_y, where $a = 5$ nm, $L = a$. It is shown that with the increase of D_y^{∞} from -15×10^{-3} C/m^2 to 15×10^{-3} C/m^2, the regularized energy release increases first and then decreases. It can be seen from the figure that the increase of positive and negative electrical loads will restrain the crack extension, which is similar to the classical piezoelectric fracture theory.[9]

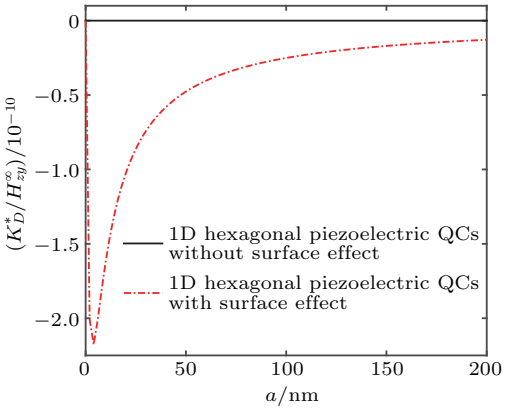

Fig. 9. Variations of K_D^*/H_{zy}^{∞} with a.

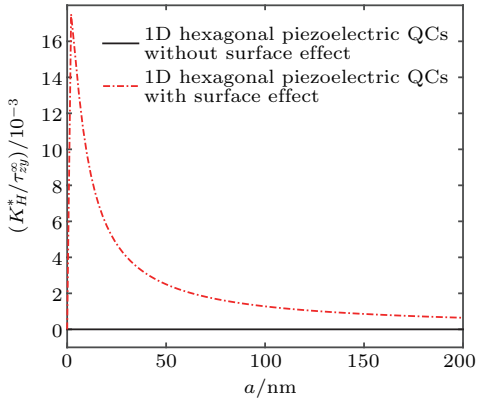

Fig. 6. Variations of K_H^*/τ_{zy}^{∞} with a.

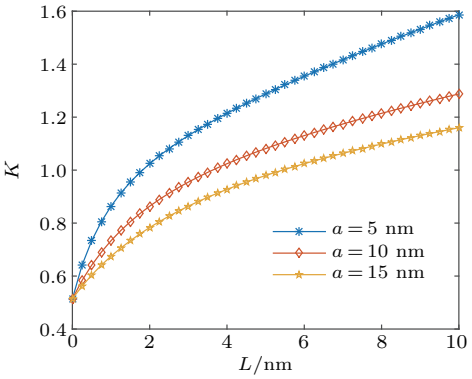

Fig. 10. Variations of K with L for some given a.

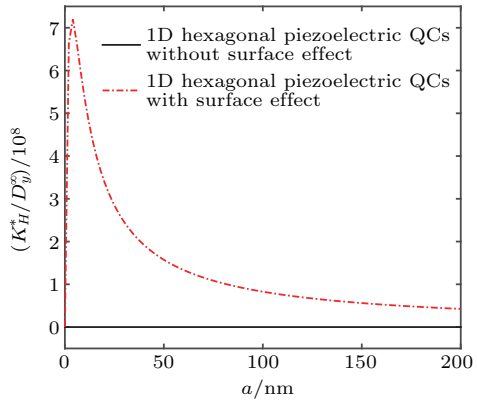

Fig. 7. Variations of K_H^*/D_y^{∞} with a.

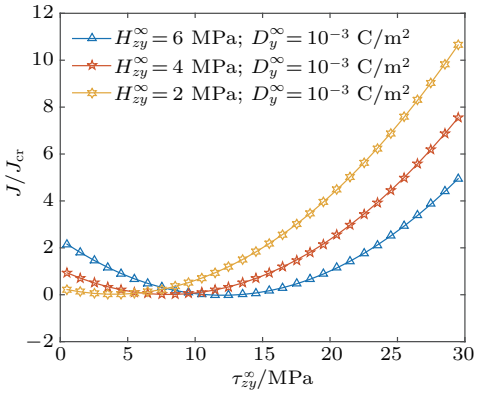

Fig. 11. Variations of $J/J_{\rm cr}$ with τ_{zy}^{∞} for some given H_{zy}^{∞}.

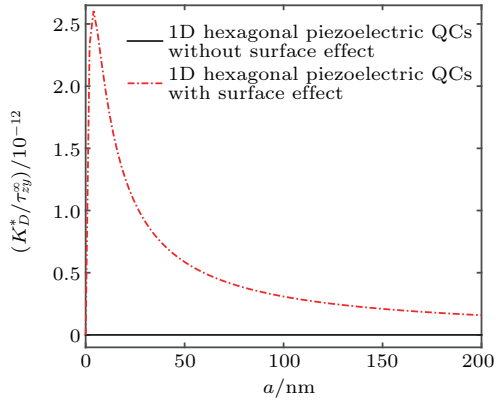

Fig. 8. Variations of K_D^*/τ_{zy}^{∞} with a.

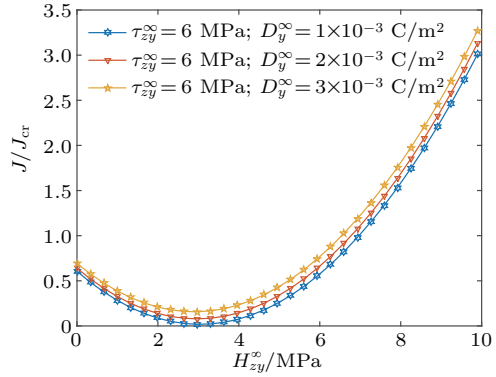

Fig. 12. Variations of $J/J_{\rm cr}$ with H_{zy}^{∞} for some given D_y^{∞}.

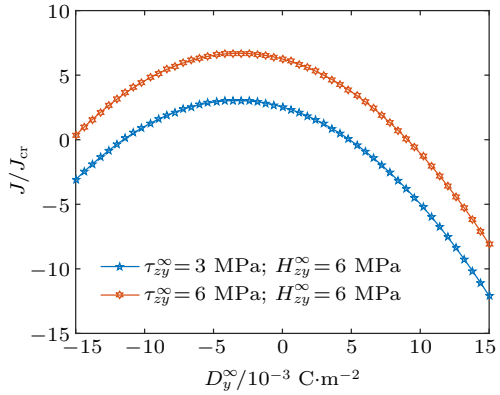

Fig. 13. Variations of $J/J_{\rm cr}$ with D_y^{∞} for some given τ_{zy}^{∞}.

6. Conclusions

Based on the theory of surface elasticity, we have studied the fracture mechanics of six edge nano-cracks emanating from regular hexagonal nano-hole in 1D hexagonal piezoelectric QCs. A new conformal mapping is constructed, and the exact solutions of stress field, electric field, stress intensity factor of crack tip, electric displacement intensity factor and energy release rate around the six edge nano-cracks emanating from regular hexagonal nano-hole are given. The analytical solution of 1D hexagonal piezoelectric QCs with six edge nano-cracks emanating from regular hexagonal nano-hole under the classical fracture theory is also obtained.

(1) Under the influence of surface effect, the stress intensity factor of the phonon field, the stress intensity factor of the phason field, the electric displacement intensity factor are all affected by the coupling of far-field stress and electrical loads. This is obviously different from the result without surface effect in 1D hexagonal piezoelectric QCs.

(2) At nanoscale, the influence of surface effect is very obvious. With the increase of the crack and hexagon side length, the influence of the surface effect decreases gradually, and the final result tends to the classical fracture theory.

(3) When the surface effect is not considered, the dimensionless field intensity factor increases with the increase of cracks. However, in a certain range, the increase of the side length of the hexagonal hole will reduce it.

(4) At nanoscale, the energy release rate decreases first and then increases with the increase of the phonon field mechanical loads and phason field mechanical loads, the increase of positive and negative electrical loads will restrain the crack extension.

Appendix A

In Ref. [10], Hou *et al.* introduced conformal mapping from the outside of regular hexagon to the outside of unit circle to construct conformal mapping, the exterior of the hexagon with six cracks was mapped to the interior of the circle with radius a. The construction process is as follows:

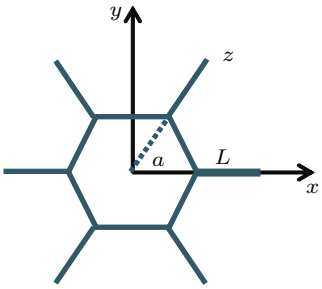

Fig. A1. z plane.

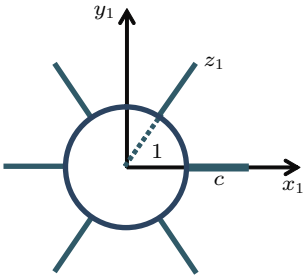

Fig. A2. z_1 plane.

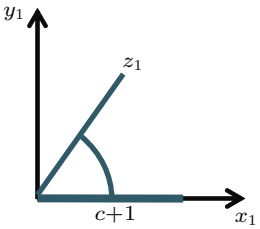

Fig. A3. z_1 plane, $0<\theta<\frac{\pi}{3}$.

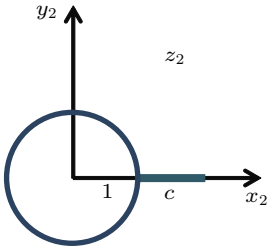

Fig. A4. z_2 plane.

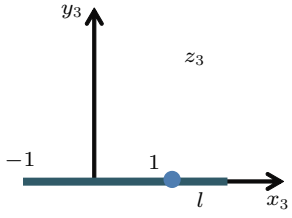

Fig. A5. z_3 plane.

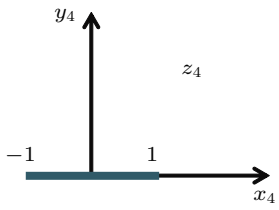

Fig. A6. z_4 plane.

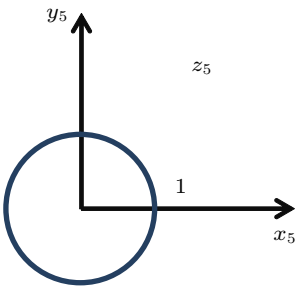

Fig. A7. z_5 plane.

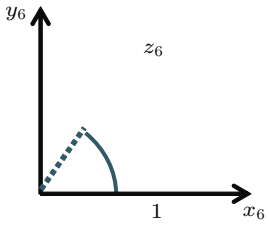

Fig. A8. z_6 plane.

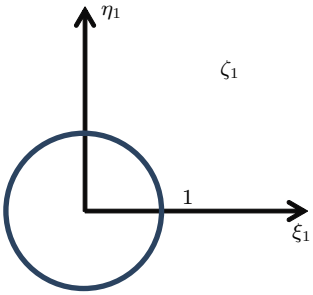

Fig. A9. ζ plane.

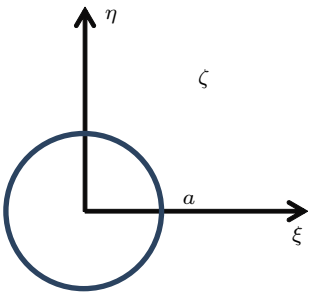

Fig. A10. ζ plane.

$$z = R[z_1 + \frac{1}{15}z_1^{-5} + \frac{1}{99}z_1^{-11} + \frac{1}{1377}z_1^{-17}], \tag{A1}$$

$$z_2 = z_1^6, \tag{A2}$$

$$z_3 = \frac{1}{2}(z_2 + \frac{1}{z_2}), \tag{A3}$$

$$z_4 = \frac{2z_2 + 1 - l}{1 + l}, \tag{A4}$$

$$z_5 = z_4 + \sqrt{z_4^2 - 1}, \tag{A5}$$

$$z_6 = z_5^{\frac{1}{6}}, \tag{A6}$$

$$\zeta_1 = \frac{1}{z_6}, \tag{A7}$$

$$\zeta = a\zeta_1, \tag{A8}$$

where $R = 0.9258a$, $l = [(1+c)^6 + (1+c)^{-6}]/2$. The positive real parameter c determined by the following formula:

$$L + a = R\Big[(1+c) + \frac{1}{15}(1+c)^{-5} + \frac{1}{99}(1+c)^{-11} + \frac{1}{1377}(1+c)^{-17}\Big]. \tag{A9}$$

From Eqs. (A2)–(A7), it is obtained that

$$z_1 = \chi(\zeta_1) = \frac{1}{2^{\frac{1}{3}}\zeta_1}[(\zeta_1^6 - 1)^2 + l(\zeta_1^6 + 1)^2 + \sqrt{1+l}(\zeta_1^6 + 1) \times \sqrt{(1+l)\zeta_1^{12} + 2(l-3)\zeta_1^6 + (1+l)}]^{\frac{1}{6}}. \tag{A10}$$

Equation (A10) provides a conformal mapping from the outside region of a unit circle with six cracks in the z_1 plane to the interior of a unit circle in the ζ_1 plane, it is consistent with the result of Ref. [8] (when $2^k = 6$, $R = 1$).

References

[1] Shechtman D, Blech I and Gratias D *et al.* 1984 *Phys. Rev. Lett.* **53** 1951
[2] Liu G T, Fan T Y and Guo R P 2003 *Mech. Res. Commun.* **30** 335
[3] Liu G T and Fan T Y 2003 *Sci. Chin. E* **46** 326
[4] Liu G T, Fan T Y and Guo R P 2004 *Int. J. Solids Struct.* **41** 3949
[5] Guo J H and Liu G T 2008 *Appl. Math. Mech-Engl.* **29** 485
[6] Guo J H and Liu G T 2007 *Acta Math. Appl. Sin.* **30** 1066 (in Chinese)
[7] Guo J H and Liu G T 2008 *Chin. Phys. B* **17** 2610
[8] Chen Z, Liu G and Guan L 2011 *Chin. J. Solid Mech.* **29** 412 (in Chinese)
[9] Zhong H Y and Liu G T 2015 *Chin. J. Solid Mech.* **36** 179 (in Chinese)
[10] Hou X L, WANG J X and Jia L G 2018 *Chin. J. Appl. Mech.* **35** 484 (in Chinese)
[11] Liu G T and Yang L Y 2017 *Chin. Phys. B* **26** 094601
[12] Li L H and Liu G T 2012 *Acta Phys. Sin.* **61** 086103 (in Chinese)
[13] Li L H and Liu G T 2009 *Mod. Phys. Lett. B* **23** 3397
[14] Wang X 2006 *Mech. Res. Commun.* **33** 576
[15] Li X, Huo H S and Shi P P 2014 *Chin. J. Solid Mech.* **35** 135
[16] Fu X L, Wang G F and Feng X Q 2010 *Eng. Fract. Mech.* **77** 1048
[17] Kim C I, Schiavone P and Ru C Q 2011 *Arch. Mech.* **63** 267
[18] Gurtin M E, Murdoch A I 1975 *Arch. Ration. Mech. Anal.* **57** 291
[19] Gurtin M E, Murdoch A I 1978 *Int. J. Solids Struct.* **14** 431
[20] Xiao J H, Xu Y L and Zhang F C 2018 *Theor. Appl. Fract. Mech.* **96** 476
[21] Guo J H and Li X F 2018 *Acta Mech.* **229** 4251
[22] Liu Y Z, Guo J H and Zhang X Y 2019 *ZAMM-Z Angew. Math. Mech.* **99** e201900043
[23] Guo J H, He L T, Liu Y Z and Li L H 2020 *Theor. Appl. Fract. Mech.* **107** 102553
[24] Song J Z, Li H, He Y Z and Ou G B 2004 *J. Harbin Eng. Univ.* **25** 558
[25] Jia L G, Sun H D and Wang C G 2012 *Eng. Mech.* **29** 147 (in Chinese)
[26] Jiang L J and Liu G T 2017 *Chin. Phys. B* **26** 044601